

Long-distance coherent coupling in a quantum dot array

F. R. Braakman¹, P. Barthelemy¹, C. Reichl², W. Wegscheider² and L. M. K. Vandersypen^{1*}

Controlling long-distance quantum correlations is central to quantum computation and simulation. In quantum dot arrays, experiments so far rely on nearest-neighbour couplings only, and inducing long-distance correlations requires sequential local operations. Here, we show that two distant sites can be tunnel-coupled directly. The coupling is mediated by virtual occupation of an intermediate site, with a strength that is controlled via the energy detuning of this site. It permits a single charge to oscillate coherently between the outer sites of a triple dot array without passing through the middle, as demonstrated through the observation of Landau-Zener-Stückelberg interference. The long-distance coupling significantly improves the prospects of fault-tolerant quantum computation using quantum dot arrays, and opens up new avenues for performing quantum simulations in nanoscale devices.

Nanofabricated circuits of quantum dot arrays provide an excellent platform for quantum information processing using single charges or spins^{1–4}. In such a dot array architecture, the tunnel coupling between neighbouring dots plays an essential role. It governs the motion of charges between the dots, permitting delocalization⁵ over the dots and coherent oscillations between them^{4–6}. Indeed, the same tunnel coupling is at the core of exchange-based quantum gates on spin qubits^{1,7,8}.

Tunnel coupling falls off exponentially with distance, and all experiments on quantum dot arrays so far rely on nearest-neighbour couplings only. Furthermore, quantum dot arrays are typically constructed from one-dimensional segments because realizing two-dimensional arrays is challenging. These restrictions severely constrain the range of experiments currently possible in this system. Instead of having to repeatedly swap neighbouring qubits down the chain, long-distance coupling would enable quantum gates between distant qubits in one step, thereby giving access to many of the benefits of a two-dimensional lattice. This would strongly reduce the requirements for fault-tolerant quantum computing^{9,10} and permit quantum simulation of phenomena that are otherwise inaccessible in this system, for instance involving frustration¹¹ or superexchange^{12,13}.

The most common approach to realizing an effective long-distance coupling is to use a quantum bus, as demonstrated for trapped ions¹⁴ and superconducting qubits^{15,16}. For quantum dots, such a bus has been proposed in the form of optical cavities¹⁷ and microwave stripline resonators^{18–20}. For the latter, first steps have been taken by demonstrating coupling between a double quantum dot and a resonator^{21,22}. Furthermore, charge transfer through a channel connecting two distant quantum dots has recently been realized using surface acoustic waves that push electrons forward^{23,24}. In this approach, charge coherence is lost, but spin coherence is expected to be preserved.

As an alternative means for creating long-distance coupling of quantum dots, and which does not require separate elements such as cavities or channels, a quantum bus has been proposed in the form of the continuum of conduction or valence band states²⁵. Through a second-order process known as co-tunnelling, virtual occupation of these states can induce an effective coupling

between distant quantum dots. Inspired by this scheme, we propose to create such long-distance coupling by virtual occupation of discrete states of quantum dots located in between. In this case, only discrete levels participate in the co-tunnelling process. This permits a fully coherent process, in contrast to all existing measurements of co-tunnelling in quantum dots, in which quantum coherence is quickly lost in the source and drain reservoirs (see ref. 26 for a review).

Here, we demonstrate the coherent transfer of single electron charges between the outer sites of a linear array consisting of three quantum dots, in a regime where sequential transport through the middle dot is energetically suppressed. Using real-time charge detection techniques, we study the dependence of the rate with which electrons hop between the outer dots on detuning of the middle dot levels. We observe a non-monotonous dependence that is characteristic of a coupling mechanism mediated by virtual occupation of the middle dot levels. We also control quantum coherent dynamics between the outer dots in the form of Landau-Zener-Stückelberg (LZS) interference, induced by a process we term photon-assisted co-tunnelling (PACT).

A scanning electron microscopy (SEM) image of a device identical to the one used is shown in Fig. 1a. Gate electrodes fabricated on the surface of a GaAs/AlGaAs heterostructure (see Methods) are biased with appropriate voltages to selectively deplete regions of the two-dimensional electron gas (2DEG) below and define the linear array of three quantum dots. In the array, only adjacent dots are connected through tunnel barriers. The left and right dots are also tunnel-coupled to the left and right reservoirs, respectively. Above the blue-shaded gate a charge sensing quantum dot (SQD) is created, the conductance of which is sensitive to the number of charges on each dot in the array through capacitive coupling. For maximum sensitivity, the SQD is operated on the flank of a Coulomb peak. Furthermore, one of the SQD contacts is connected via a bias-tee to an LC-circuit so that the SQD conductance can be measured both by radiofrequency (RF) reflectometry²⁷ and in direct current (d.c.) transport measurements (see Methods).

We operate the device in the few-electron regime. By sweeping the voltages on gates LP, MP and RP (Fig. 1a), the number of electrons on each of the dots of the triple dot array can be changed one

¹Kavli Institute of Nanoscience, TU Delft, 2600 GA Delft, The Netherlands, ²Solid State Physics Laboratory, ETH Zürich, 8093 Zürich, Switzerland.

*e-mail: l.m.k.vandersypen@tudelft.nl

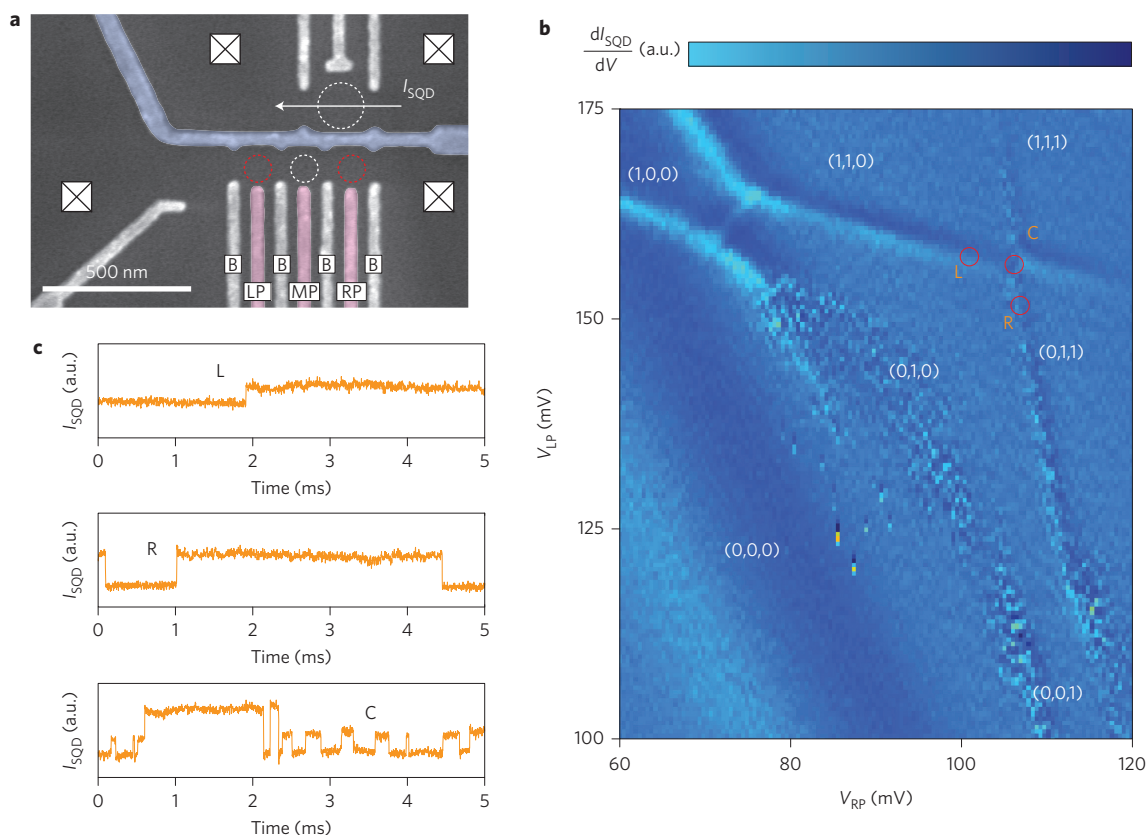


Figure 1 | Linear array of three quantum dots and real-time tunnelling measurements. **a**, SEM image of a sample identical to the one used for the measurements. Dotted circles indicate quantum dots, squares indicate Fermi reservoirs in the 2DEG, which are contacted through ohmic contacts. Both the current through (white arrow) and the reflectance of the SQD are monitored and used to determine the occupancies of the triple quantum dot. **b**, Numerical derivative (along the V_{LP} axis) of current through the SQD as a function of the voltages on gates LP and RP, mapping out a charge stability diagram of the triple dot in the few-electron regime. The $(0,0,0)$ – $(0,1,0)$ charging transition appears fragmented because of low tunnelling rates from the reservoirs to the centre dot. **c**, Real-time traces of the sensing dot reflectometry signal, taken at points L, R and C as indicated in **b**. We use a 50 kHz low-pass filter (Avens Signal Equipment AP220) to filter the reflectometry signal to obtain sufficient signal-to-noise.

by one. A time-averaged measurement of the differential d.c. conductance through the SQD as a function of V_{LP} and V_{RP} maps out a cross-section of the three-dimensional charge stability diagram of the triple dot (Fig. 1b). The occupancy is denoted here as (n,m,p) , corresponding to the number of electrons on the left, middle and right dots, respectively.

The strength of the four tunnel couplings can be tuned individually with the voltages on the barrier gates (labelled B in Fig. 1a). The tunnel rates between the outer dots and their respective leads are set to the 100 Hz range. The tunnel rates between neighbouring sites are tuned to be much higher. The upper two panels of Fig. 1c show real-time traces of the charge detector RF reflectometry signal taken at points R and L in the charge stability diagram (Fig. 1b). The first trace shows a single step corresponding to the transfer of one electron from the left dot to the left reservoir, that is, going from $(1,1,0)$ to $(0,1,0)$. In the second trace, three single-electron tunnel events are seen, once from the right dot to the right reservoir and twice the other way, that is, alternating between $(0,1,1)$ and $(0,1,0)$. The step size is larger than in the first trace because of the closer proximity of the SQD to the right dot than to the left dot.

Remarkably, when we consider point C in the charge stability diagram, the real-time trace (lower panel) not only shows steps corresponding to the slow tunnelling between outer dots and leads, but also exhibits smaller steps that occur at a rate that is an order of magnitude higher. Because point C is at the boundary of the $(1,1,0)$ or $(0,1,1)$ regions in the charge stability diagram, the fast steps

appear to correspond to single electron transfers between the outer two dots. This is consistent with the step size, as well as with the observation that the mean times over which the measured conductance is high or low are equal for zero detuning between $(1,1,0)$ and $(0,1,1)$ (point C). Upon increasing or decreasing the detuning, these times quickly become unequal (Supplementary Section S2).

This tunnelling between the left and right dots is at first sight unexpected, because in these measurements the centre dot levels are far detuned from resonance with the outer dot levels, excluding sequential tunnelling via the centre dot (there is no charging line of the centre dot present nearby in the charge stability diagram). We argue that these tunnelling events are transfers of single electrons between the outer dots, via virtual occupation of the middle dot^{27,28}. This implies that electrons are transferred between the outer parts of the array, essentially without passing through the dot in between.

This tunnelling between remote dots can be seen for different charge configurations of the triple dot array. Here, we focus on transitions between $(1,1,0)$ and $(0,1,1)$. In this case, two virtual pathways exist for the transfer: either a single electron first moves virtually from the left to the middle dot and then from the middle to the right dot, or an electron moves first from middle to right and then another electron moves from left to middle (note that for other charge configurations the situation can be different; for instance for tunnelling between $(1,0,0)$ and $(0,0,1)$, only the first pathway exists). As will be shown in the following, the existence

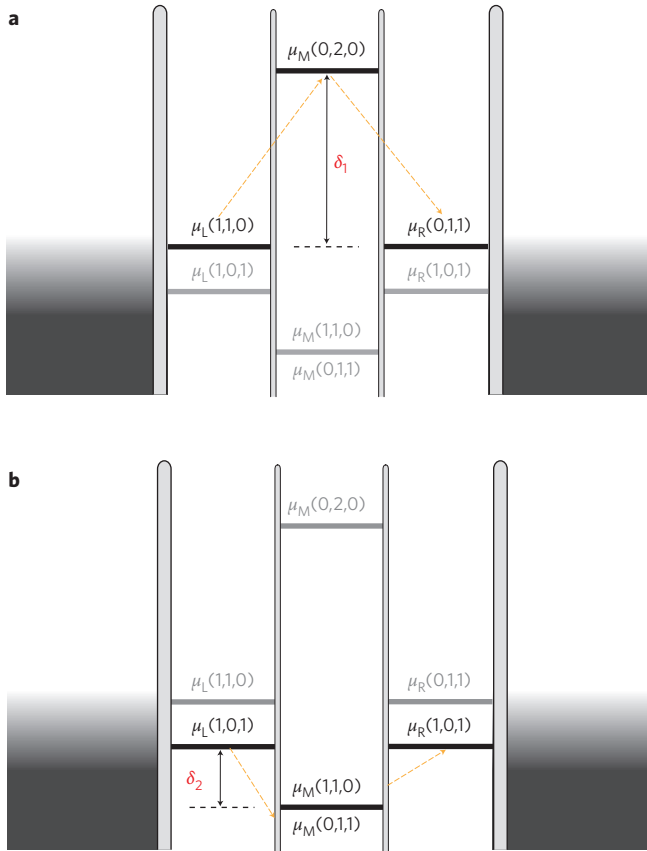


Figure 2 | Co-tunnelling between outer dots. **a,b**, Schematic representations of the co-tunnelling process in terms of the relevant electrochemical potentials in the linear dot array. The two panels illustrate the two possible pathways for co-tunnelling between $|110\rangle$ and $|011\rangle$, as explained in the main text.

of two virtual pathways makes the transfer rate depend non-monotonously on the detuning between the intermediate virtual states and the initial and final states. The dependence on middle dot detuning is a key signature of this process.

The charge transfer is depicted schematically in Fig. 2a,b. Because it involves removing an electron from one dot and adding it to another dot, we need to compare electrochemical potentials for the transitions between initial, intermediate virtual and final charge states. Only ground-state to ground-state transitions are considered. We denote the various electrochemical potentials as

$$\mu_L(n, m, p) = E(n, m, p) - E(n-1, m, p)$$

$$\mu_M(n, m, p) = E(n, m, p) - E(n, m-1, p)$$

$$\mu_R(n, m, p) = E(n, m, p) - E(n, m, p-1)$$

for the left, middle and right dots, respectively. Here, $E(n, m, p)$ stands for the ground-state energy of a given charge configuration (n, m, p) . For the transition back and forth between states $|110\rangle$ and $|011\rangle$ to occur spontaneously, we require $\mu_L(1,1,0) = \mu_R(0,1,1)$ (we denote the lowest energy state with occupation (n, m, p) as $|nmp\rangle$). Furthermore, to quantify the detuning between virtual states, and initial and final states, we introduce two parameters, δ_1 and δ_2 . For charge transfer via virtual occupation of $|020\rangle$, the relevant detuning parameter is $\delta_1 = \mu_M(0,2,0) - \mu_L(1,1,0)$ (Fig. 2a). For charge transfer via $|101\rangle$, the relevant detuning is

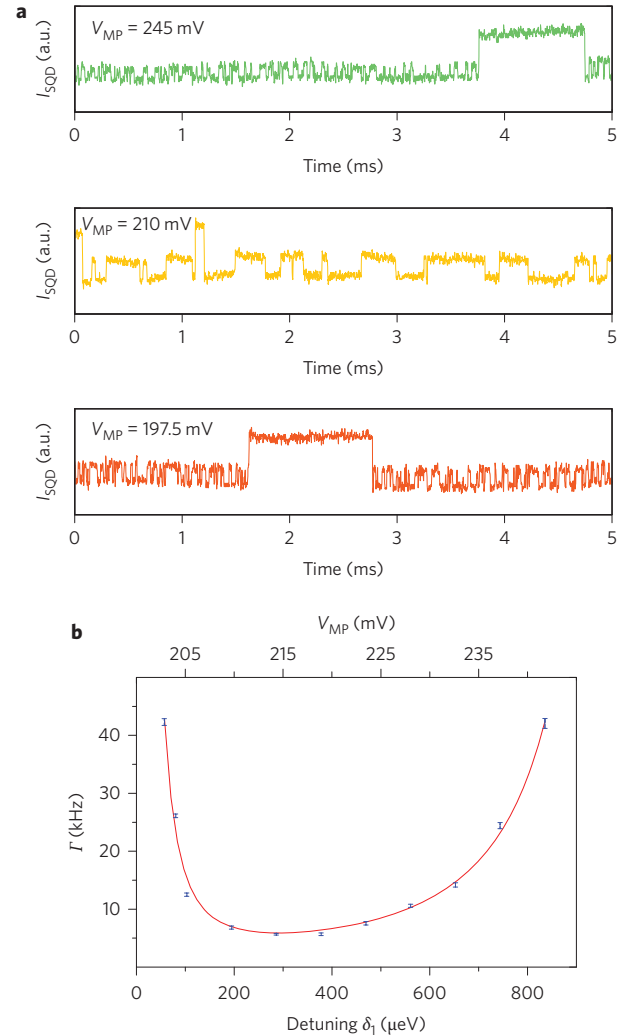


Figure 3 | Real-time tunnelling. **a**, Real-time traces of the SQD reflectometry signal, taken at zero detuning between the outer dot levels, for three values of V_{MP} corresponding to three values of δ_1 and δ_2 . **b**, Plot of the measured co-tunnelling rate Γ versus detuning δ_1 . The non-monotonous dependence is a clear indication that the transfer proceeds via co-tunnelling. This is corroborated by the fact that the measured data points can be fitted well with the predicted expression for Γ (red curve). To make the fit, we rewrite equation (1) as $\Gamma = a/\delta_1^2 + b/(c - d\delta_1)^2$, where a , b , c and d are positive constants. For the detuning axis, gate voltages are converted to energies using microwave-induced sidebands as an energy reference (Supplementary Section S6). The error bars on the obtained values for Γ include errors associated with the threshold analysis of the real-time traces (low-frequency noise modulates the baseline signal, so the precise value of the threshold slightly affects the statistics) and sampling errors due to the finite number of transfer events per trace²⁹ (we sample over 100 ms traces). Note that the use of a low-pass filter results in an overall underestimation of Γ .

$\delta_2 = \mu_L(1,0,1) - \mu_M(1,1,0)$ (Fig. 2b). Note that δ_1 and δ_2 are related and cannot be changed independently, as V_{MP} increases δ_1 by the same amount it decreases δ_2 . The total tunnel rate Γ is the sum of the tunnel rates via the two respective paths. It can be expressed as (Supplementary Section S5)

$$\Gamma = \frac{2T_2}{\hbar} \left(\frac{t_{11}^2 t_{r1}^2}{\delta_1^2} + \frac{t_{12}^2 t_{r2}^2}{\delta_2^2} \right) \quad (1)$$

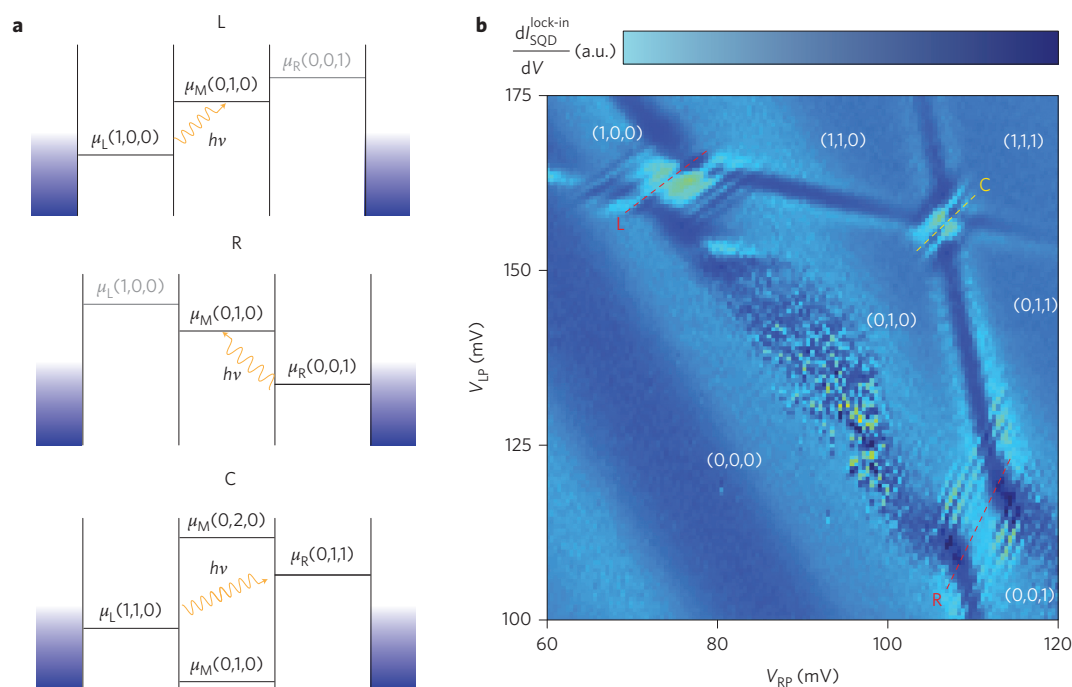


Figure 4 | Microwave-driven transitions. **a**, Schematic view of PAT processes between different pairs of dots. Charges can be transferred from one dot to another when the detuning between the corresponding electrochemical potentials matches the photon energy. The left and middle panels correspond to PAT, and the right panel corresponds to PACT. Note that similar resonances to the ones shown exist for negative detunings. **b**, Charge stability diagram in the same configuration as in Fig. 1b, but now with microwave excitation (15 GHz) applied via a bias-tee to gate LP. The microwaves were chopped at the reference frequency of a lock-in amplifier and combined with a small-amplitude modulation of the same reference frequency. The colourscale data are the numerical derivative (along the V_{LP} axis) of the SQD signal acquired via the lock-in amplifier. Multiple sidebands develop where PAT or PACT occurs.

Here t_{11} , t_{r1} , t_{12} and t_{r2} are the tunnel coupling elements between $|110\rangle$ and $|020\rangle$, $|020\rangle$ and $|011\rangle$, $|101\rangle$ and $|011\rangle$, and $|110\rangle$ and $|101\rangle$, respectively. The charge dephasing time T_2 is assumed to be much smaller than $1/\Gamma$ (T_2 is typically ~ 1 ns (refs 4, 6), so interference effects between the two pathways can be neglected). Equation (1) is valid as long as the four tunnel couplings and the detuning between $|110\rangle$ and $|011\rangle$ are small compared to δ_1 and δ_2 .

We experimentally verify the non-monotonous dependence of Γ on detuning δ_1 (and hence δ_2) by stepping the voltage on gate MP (V_{MP}) and measuring the rate of tunnelling between $|110\rangle$ and $|011\rangle$. Figure 3a presents three traces, each for a different value of V_{MP} . For the top trace the value of V_{MP} corresponds to small δ_1 and large δ_2 , so the transfer proceeds mainly as depicted in Fig. 2a. For the middle trace, V_{MP} is set such that both δ_1 and δ_2 are relatively large, resulting in a reduced, but non-zero tunnel rate, in agreement with equation (1). Finally, for the lower trace, δ_2 is small and δ_1 is large. In this case, tunnelling proceeds mainly via the virtual process shown in Fig. 2b and the tunnel rate is higher again.

For a quantitative analysis, we extract the tunnel rate Γ from real-time traces such as in Fig. 3a using the relation²⁹ $\Gamma^{-1} = f(1-f)(\langle\tau_L\rangle + \langle\tau_R\rangle)$, where f is the Fermi probability distribution. Times $\langle\tau_L\rangle$ and $\langle\tau_R\rangle$ are the average times between tunnel events spent in the left and right dot, respectively. We perform a threshold analysis of the real-time traces to obtain the distributions of τ_L and τ_R . The value of f can be established using the relation $f = \langle\tau_L\rangle / (\langle\tau_L\rangle + \langle\tau_R\rangle)$. Figure 3b shows measured values of Γ determined in this way, for different values of the detuning, parametrized by δ_1 . The non-monotonous dependence is striking and is fit well by equation (1) (red curve, Fig. 3b), implying that the transfer indeed proceeds via virtual occupation of intermediate states.

The hopping of electrons between the outer sites in the array indicates that an effective tunnel coupling is present between the left and right dot, which we call co-tunnel coupling. We can express the

strength of this co-tunnel coupling as (Supplementary Section S3)

$$t_{co} = \frac{t_{11}t_{r1}}{\delta_1} + \frac{t_{12}t_{r2}}{\delta_2}$$

We note that t_{co} need not be small: for typical experimental values of the nearest-neighbour tunnel couplings of order $10 \mu\text{eV}$ and for detunings of $\sim 100 \mu\text{eV}$, we obtain $t_{co} \approx 1 \mu\text{eV}$. The co-tunnel coupling enters the Hamiltonian in much the same way as the direct tunnel coupling between neighbouring sites, so many phenomena arising from direct tunnel coupling have their counterpart in co-tunnel coupling between remote sites. For instance, on application of microwave excitation to a gate, direct tunnel coupling can give rise to photon-assisted tunnelling (PAT). In complete analogy, we can expect a photon-assisted version of the co-tunnelling process described above, which we term photon-assisted co-tunnelling (PACT).

PAT is a well-described phenomenon in quantum dots and has been observed many times in single and tunnel-coupled double quantum dots^{5,30}. Tunnelling transitions of electrons between two detuned neighbouring dots can be made resonant by applying microwaves of a frequency matching the detuning, $\varepsilon_0 = nh\nu$ (Fig. 4a). Here, ε_0 is the detuning, ν is the microwave frequency, and n is an integer, with $n > 1$ corresponding to multiphoton resonances.

We apply microwave excitation at $\nu = 15$ GHz to gate LP. The microwaves are chopped at the reference frequency of a lock-in amplifier (see Methods). The excitation introduces a number of sidebands in the charge stability diagram. Two sets of sidebands are due to conventional PAT between neighbouring tunnel-coupled quantum dots. They are seen in Fig. 4b near the $|100\rangle$ to $|010\rangle$ transition (point L) and $|001\rangle$ to $|010\rangle$ transition (point R). The slope of these lines is such that $\varepsilon_0 = nh\nu$ is maintained.

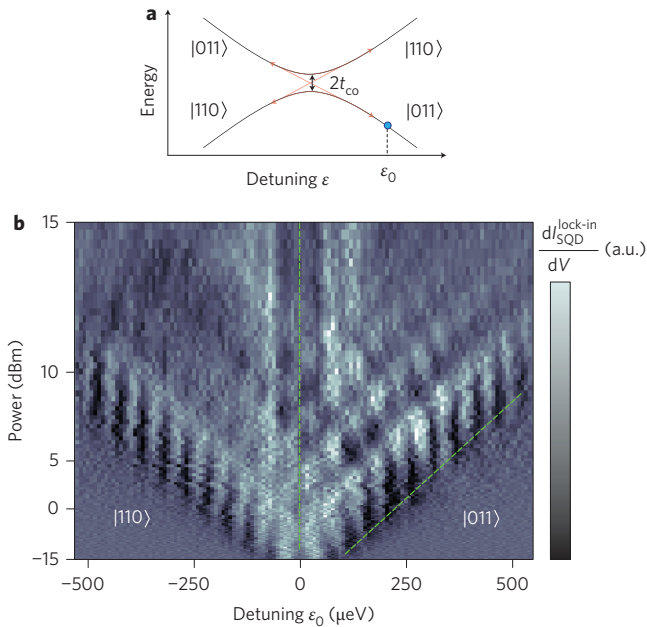


Figure 5 | LZS interference. **a**, Schematic energy level diagram as a function of detuning between $|110\rangle$ and $|011\rangle$, displaying an avoided crossing due to co-tunnel coupling. Red arrows represent the response of the system to microwaves modulating the detuning. Multiple passings of the avoided crossing result in quantum interference of the two paths. **b**, Numerical derivative (along the detuning axis) of the lock-in signal of I_{SQD} (as in Fig. 4b) as a function of detuning and microwave power. LZS interference fringes are clearly visible along both axes.

Near the $|110\rangle$ to $|011\rangle$ transition (point C), a different set of resonances develop. Based on their slope and location, we identify these transitions to occur via PACT, where single electrons tunnel between the outer dots, now assisted by the microwave excitation. As expected for photon-assisted processes, these resonances appear at a detuning that is linearly dependent on the microwave frequency (Supplementary Section S7).

To achieve a strong PACT response, the tunnel couplings between neighbouring dots are set to a much higher value than in the real-time experiment already described. We can extract the nearest-neighbour tunnel couplings from the spacing between the PAT resonances along the detuning axis as a function of frequency^{5,29} (Supplementary Section S7) and find $8.1 \pm 0.4 \mu\text{eV}$ for the tunnel coupling between right and centre dots, and $12.3 \pm 0.3 \mu\text{eV}$ between left and centre dots.

Importantly, photon-assisted co-tunnelling allows us to demonstrate the coherent dynamics driven by the co-tunnel coupling, through the observation of LZS interference³¹. Coherent quantum dynamics in the form of LZS interference has been observed in a wide range of two-level quantum systems, such as electronic states of atoms and molecules^{32,33} or superconducting devices³⁴, and spin states in double quantum dots³⁵. In LZS interferometry, a two-level system is swept through an anticrossing of its levels at such a rate that a superposition of its ground and excited states is reached (Fig. 5a). Between two passings through the anticrossing (at times t_1 and t_2), the two parts of the superposition acquire a relative phase due to their difference in energy ε ,

$$\Delta\Theta_{12} = \frac{1}{\hbar} \int_{t_1}^{t_2} \varepsilon(t) dt$$

At the second passing through the anticrossing, the two paths in phase space will interfere. Destructive interference in the occupation

probability of the excited state occurs for $\Delta\Theta_{12} = (2n + 1)\pi$, where n is an integer.

In our experiment, the applied microwaves modulate the detuning ε between $\mu_L(1,1,0)$ and $\mu_R(0,1,1)$. This takes the system back and forth through the anticrossing created by the co-tunnel coupling (Fig. 5a). The amplitude of the microwaves is used to control the value of $\Delta\Theta_{12}$ (ref. 34). Figure 5b shows a measurement of the SQD signal as a function of detuning ε_0 versus microwave power. Contrast against the background indicates a finite population in the excited state (the ground-state configuration for positive and negative detuning is as indicated in Fig. 5b). We see that for both positive and negative detunings, the excited-state population exhibits interference fringes when sweeping the power (moving along the vertical dashed line). The oscillations indicate that a coherent superposition of $|110\rangle$ and $|011\rangle$ is created and maintained between subsequent passings through the anticrossing.

Because the microwaves periodically drive the system through the anticrossing, multiple crossings also need to be considered. Consecutive cycles interfere constructively when the total phase difference accumulated over one complete microwave period $\Delta\Theta_{\text{tot}}$ equals $2\pi n$. As

$$\Delta\Theta_{\text{tot}} = (1/\hbar) \int \varepsilon(t) dt = 2\pi\varepsilon_0/h\nu$$

this causes peaks to appear for detunings $\varepsilon_{0,n} = nh\nu$. This can be clearly seen in Fig. 5b, where along the horizontal direction ten fringes can be discerned.

In summary, we have demonstrated an effective coherent co-tunnel coupling between the outer dots in a triple quantum dot, which is mediated by virtual occupation of levels on the middle dot. The coupling strength can be controlled via detuning between the relevant middle and outer dot levels and agrees well with theoretical predictions.

The long-distance tunnel coupling may also be used for realizing spin exchange gates, at a distance, in one step. When the intermediate site is itself occupied by an electron, its spin affects the strength of the co-tunnel coupling due to the Pauli exclusion principle, introducing correlations between the middle spin and the outer spins (that is, it realizes a three-qubit gate). The first schemes for avoiding these correlations have been worked out, enabling direct long-distance spin exchange also for this scenario (P. Stano and D. Loss, personal communication). Furthermore, the co-tunnel coupling can be extended to include multiple intermediate sites. Long-distance coupling thus provides a new approach for operating quantum circuits based on quantum dot qubits, which eases the requirements for fault tolerance. The co-tunnel coupling observed here also gives access to a new range of phenomena with interacting spins, such as superexchange^{12,13} and frustration¹¹, which can serve as a starting point for quantum simulations.

Methods

The experiment was performed on a GaAs/Al_{0.25}Ga_{0.75}As heterostructure grown by molecular-beam epitaxy, with 85-nm-deep 2DEG with an electron density of $2.0 \times 10^{11} \text{ cm}^{-2}$ and mobility of $5.6 \times 10^6 \text{ cm}^2 \text{ V}^{-1} \text{ s}^{-1}$ at 4 K. The metallic (Ti–Au) surface gates were fabricated using electron-beam lithography. The device was cooled inside an Oxford AST Sorb dilution refrigerator to a base temperature of $\sim 55 \text{ mK}$. To reduce charge noise³⁶, the sample was cooled while applying a positive voltage bias on all gates (ranging between 200 and 350 mV). The magnetic field, as well as the bias across the linear triple quantum dot, were set to zero throughout the experiment. Gates LP and RP were connected to homebuilt bias-tees, enabling application of d.c. as well as high-frequency voltage bias to these gates. RF reflectometry of the SQD was performed using an LC circuit matching a carrier wave of frequency 193.35 MHz. The power of the carrier wave arriving at the sample was about -84 dBm . The reflected signal was amplified using a cryogenic Quinstar QCA-U-219-33H amplifier and subsequently demodulated using homebuilt electronics. A Stanford Research Systems SR830 lock-in amplifier was utilized in some of the measurements. In these measurements, a square-wave modulation of amplitude 2 mV, before 16 dB attenuation, was applied to gate LP at a lock-in reference frequency of 3,412 Hz. For the microwave measurements, this square wave

was combined with the microwaves, chopped at the same reference frequency. The microwaves were generated by an Agilent E8267D microwave source.

Received 11 January 2013; accepted 19 March 2013;
published online 28 April 2013

References

- Loss, D. & DiVincenzo, D. P. Quantum computation with quantum dots. *Phys. Rev. A* **47**, 120–126 (1998).
- Taylor, J. M. *et al.* Fault-tolerant architecture for quantum computation using electrically controlled semiconductor spins. *Nature Phys.* **1**, 177–183 (2005).
- Hanson, R., Kouwenhoven, L. P., Petta, J. R., Tarucha, S. & Vandersypen, L. M. K. Spins in few-electron quantum dots. *Rev. Mod. Phys.* **79**, 1217–1265 (2007).
- Hayashi, T., Fujisawa, T., Cheong, H. D., Jeong, Y. H. & Hirayama, Y. Coherent manipulation of electronic states in a double quantum dot. *Phys. Rev. Lett.* **91**, 226804 (2003).
- Oosterkamp, T. H. *et al.* Microwave spectroscopy of a quantum-dot molecule. *Nature* **395**, 873–876 (1998).
- Petta, J. R., Johnson, A. C., Marcus, C. M., Hanson, M. P. & Gossard, A. C. Manipulation of a single charge in a double quantum dot. *Phys. Rev. Lett.* **93**, 186802 (2004).
- Petta, J. R. *et al.* Coherent manipulation of coupled electron spins in semiconductor quantum dots. *Science* **309**, 2180–2184 (2005).
- Nowack, K. C. *et al.* Single-shot correlations and two-qubit gate of solid-state spins. *Science* **333**, 1269–1272 (2011).
- Fowler, A. G., Stephens, A. M. & Groszkowski, P. High-threshold universal quantum computation on the surface code. *Phys. Rev. A* **80**, 052312 (2009).
- Stephens, A. M. & Evans, Z. W. E. Accuracy threshold for concatenated error detection in one dimension. *Phys. Rev. A* **80**, 022313 (2009).
- Kim, K. *et al.* Quantum simulation of frustrated Ising spins with trapped ions. *Nature* **465**, 590–593 (2010).
- Recher, P., Loss, D. & Levy, J. in *Macroscopic Quantum Coherence and Quantum Computing* 293–306 (Kluwer Academic, 2001).
- Mattis, D. C. *The Theory of Magnetism made Simple* (World Scientific, 2006).
- Schmidt-Kaler, F. *et al.* Realization of the Cirac–Zoller controlled-NOT quantum gate. *Nature* **422**, 408–411 (2003).
- Majer, J. *et al.* Coupling superconducting qubits via a cavity bus. *Nature* **449**, 443–447 (2007).
- Sillanpää, M. A., Park, J. I. & Simmonds, R. W. Coherent quantum state storage and transfer between two phase qubits via a resonant cavity. *Nature* **449**, 438–442 (2007).
- Imamoglu, A. *et al.* Quantum information processing using quantum dot spins and cavity QED. *Phys. Rev. Lett.* **83**, 4204–4207 (1999).
- Taylor, J. M. & Lukin, M. D. Cavity quantum electrodynamics with semiconductor double-dot molecules on a chip. Preprint at <http://arxiv.org/abs/cond-mat/0605144v1> (2006).
- Burkard, G. *et al.* & Imamoglu, A. Ultra-long-distance interaction between spin qubits. *Phys. Rev. B* **74**, 041307(R) (2006).
- Trif, M., Golovach, V. N. & Loss, D. Spin dynamics in InAs nanowire quantum dots coupled to a transmission line. *Phys. Rev. B* **77**, 045434 (2008).
- Frey, T. *et al.* Dipole coupling of a double quantum dot to a microwave resonator. *Phys. Rev. Lett.* **108**, 046807 (2012).
- Petersson, K. D. *et al.* Circuit quantum electrodynamics with a spin qubit. *Nature* **490**, 380–383 (2012).
- Hermelin, S. *et al.* Electrons surfing on a sound wave as a platform for quantum optics with flying electrons. *Nature* **477**, 435–438 (2011).
- McNeil, R. P. G. *et al.* On-demand single-electron transfer between distant quantum dots. *Nature* **477**, 439–442 (2011).
- Trauzettel, B., Bulaev, D. V., Loss, D. & Burkard, G. Spin qubits in graphene quantum dots. *Nature Phys.* **3**, 192–196 (2007).
- Ihn, T. *Semiconductor Nanostructures: Quantum states and Electronic Transport* (Oxford Univ. Press, 2010).
- Reilly, D. J., Marcus, C. M., Hanson, M. P. & Gossard, A. C. Fast single-charge sensing with a rf quantum point contact. *Appl. Phys. Lett.* **91**, 162101 (2007).
- Busl, M. *et al.* Bipolar spin blockade and coherent state superpositions in a triple quantum dot. *Nature Nanotech.* **8**, 261–265 (2013).
- Gustavsson, S. *et al.* Electron counting in quantum dots. *Surf. Sci. Rep.* **64**, 191–232 (2009).
- Van der Wiel, W. G. *et al.* Electron transport through double quantum dots. *Rev. Mod. Phys.* **75**, 1–22 (2003).
- Shevchenko, S. N., Ashhab, S. & Nori, F. Landau–Zener–Stückelberg interferometry. *Phys. Rep.* **492**, 1–30 (2010).
- Child, M. S. *Molecular Collision Theory* (Dover Publications, 1974).
- Nikitin, E. E. & Umanski, S. Y. *Theory of Slow Atomic Collisions* (Springer, 1984).
- Oliver, W. D. *et al.* Mach–Zehnder interferometry in a strongly driven superconducting qubit. *Science* **310**, 1653–1657 (2005).
- Petta, J. R., Lu, H. & Gossard, A. C. A coherent beam splitter for electronic spin states. *Science* **327**, 669–672 (2010).
- Pioro-Ladrière, M. *et al.* Origin of switching noise in GaAs/Al_xGa_{1-x}As lateral gated devices. *Phys. Rev. B* **72**, 115331 (2005).

Acknowledgements

The authors acknowledge discussions with T. Baart, R. Hanson, E. Kawakami, L. Kouwenhoven, Y. Nazarov, G. Platero, P. Scarlino and M. Shafiei, and thank A. van der Enden, J. Haanstra, R. Roeleveld and R. Schouten for technical support. This work is supported by the Stichting voor Fundamenteel Onderzoek der Materie (FOM), The Netherlands Organization for Scientific Research (NWO), the Office of the Director of National Intelligence, Intelligence Advanced Research Projects Activity (IARPA), through the US Army Research Office (grant W911NF-12-1-0354), the European Office of Aerospace Research and Development (EOARD) and the Swiss National Science Foundation.

Author contributions

F.R.B. performed the experiment. C.R. and W.W. grew the heterostructure. F.R.B. fabricated the sample. F.R.B. and P.B. carried out the data analysis. F.R.B., P.B. and L.M.K.V. contributed to interpretation of the data and commented on the manuscript. F.R.B. and L.M.K.V. wrote the manuscript.

Additional information

Supplementary information is available in the [online version](#) of the paper. Reprints and permissions information is available online at www.nature.com/reprints. Correspondence and requests for materials should be addressed to L.M.K.V.

Competing financial interests

The authors declare no competing financial interests.